ECLÉTICA QUÍMICA

Eclet. Quim. 51 | e-1662, 2026

Original Articles in Chemistry and Related Areas

https://doi.org/10.26850/1678-4618.eq.v51.2026.e1662

Heavy trivalent lanthanides and yttrium *p*-aminobenzoate complexes: synthesis, thermoanalytical and spectroscopic study

José Augusto **Teixeira**[1+], Ana Paula Segantin Gaspari **Giovanini**[1], Guilherme **Isquibola**[2], Flávio Junior **Caires**[3]

Abstract

Heavy trivalent lanthanide and yttrium complexes with *p*-aminobenzoate were synthesized and characterized using thermoanalytical, spectroscopic, and complementary techniques. The results provide in-depth knowledge, particularly regarding the thermal behavior of these complexes, which had not been previously reported. Analytical and thermoanalytical data showed that the complexes exhibit a 1:3 metal-to-p-ABA stoichiometry, and FTIR spectra indicated coordination through the carboxylate and amino groups for the Ho(III)-Yb(III), and Y(III) complexes, whereas the lutetium complex showed coordination only by carboxylate group. The complexes exhibited a crystalline structure and, except the lutetium complex, were monohydrated. Simultaneous Thermogravimetric and Differential Thermal Analysis (TG-DTA) and Evolved Gas Analysis (EGA) results allowed investigation of the thermal behavior of the complexes under pyrolytic and oxidative atmospheres. EGA identified CO_2, CO, and NH_3 as the main gaseous products released during thermal decomposition in an air atmosphere, while aniline, CO_2, CO, and NH_3 were identified under a nitrogen atmosphere. Differential Scanning Calorimetry (DSC) enabled the determination of dehydration enthalpies and the study of phase transitions for the Ho(III), Er(III), and Y(III) complexes.

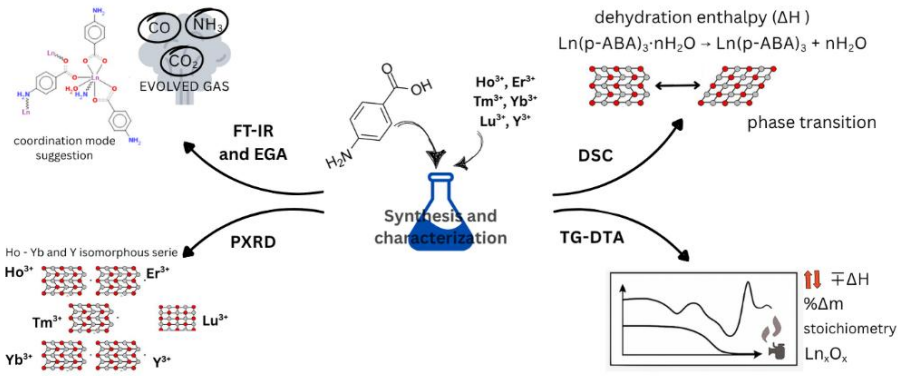

Article History

Received April 24, 2025
Accepted July 24, 2025
Published September 01, 2026

Keywords

1. p-aminobenzoate complexes
2. heavy trivalent lanthanides
3. thermoanalytical study
4. thermal decomposition
5. phase transition

Section Editors

Assis Vicente **Benedetti**

Highlights

- Coordination occurs through N/O donor atoms, except for the Lu complex.
- Unreported data on the thermal behavior of the compounds is shown for the first time.
- TG-DSC/FTIR identified H_2O, aniline, CO, CO_2 and NH_3 during thermal decomposition.
- The metal– p-ABA stoichiometry of the compounds was determined by TG–DSC.

[1]Federal Institute of Education, Science and Technology of Paraná, Paranavaí, Brazil. [2]São Paulo State University, Institute of Chemistry, Araraquara, Brazil. [3]São Paulo State University, School of Science, Bauru, Brazil. **+Corresponding author:** José Augusto Teixeira, **Phone:** +55 16 98178-0789, **Email address:** jose.teixeira@ifpr.edu.br

1. Introduction

The synthesis and study of coordination compounds have gained prominence in several research fields, mainly due to their unique properties and the broad range of possible synthetic routes (Kalembkiewicz *et al.*, 2017; Olanrewaju *et al.*, 2018). In particular, the formation of coordination complexes involving rare earth elements has been extensively investigated, primarily due to the spectroscopic properties and coordination behavior of these cations, allowing their application in diverse fields such as luminescence, healthcare, sensors, optoelectronic devices, and more (Jesty *et al.*, 2017; Zhai *et al.*, 2015).

4-Aminobenzoic acid (also known as *p*-aminobenzoic acid, H-pABA) consists of a benzene ring substituted with amino and carboxyl groups in its structure, with the molecular formula $C_7H_7NO_2$ (Kalembkiewicz *et al.*, 2017). It belongs to the Vitamin B group, a class of water-soluble compounds. H-pABA is a known derivative of naturally occurring aromatic amino acids (Samsonowicz *et al.*, 2005) and plays a key role in the biosynthesis of folic acid in bacteria and plants. It performs essential metabolic functions such as DNA replication and the synthesis of nucleotides, vitamins, and amino acids (LeBlanc *et al.*, 2013). However, H-pABA is not synthesized by mammals, and supplementation occurs through dietary intake or bacterial production, particularly by *Escherichia coli* (Koma *et al.*, 2014; Sowinska *et al.*, 2019).

In this context, H-pABA and its derivatives have received significant attention from the pharmaceutical industry (Sapijanskaitė-Banevič *et al.*, 2021), which has investigated several of its biological functions, including antioxidant (Galbinur *et al.*, 2009), antibacterial (Horozić *et al.*, 2019), anticoagulant (used as an antithrombotic drug), fibrinolytic, and immunomodulatory activities (Akberova, 2002). Recently, Aquaroni and collaborators (2020) proposed the synthesis of a new silver complex with 4-aminobenzoic acid, which exhibited antibacterial and antiproliferative activities.

As previously stated, the use of H-pABA in the construction of coordination compounds is facilitated by the presence of functional groups in its structure (specifically, the carboxylic acid and amino groups), which can act as both electron donors and acceptors, coordinating with various cations (Rosbottom *et al.*, 2017). Due to these properties, its use in coordination chemistry has been widely studied (Kalembkiewicz *et al.*, 2017).

In a recent study by our group, some alkaline earth metal complexes of *p*-aminobenzoate (the ionized form of H-pABA) were synthesized using Mg(II), Ca(II), Sr(II), and Ba(II) (Teixeira *et al.*, 2022). *p*-ABA has also been employed as a ligand in the synthesis of complexes with both divalent (Mn(II), Co(II), Ni(II), Cu(II), and Zn(II)) and trivalent metal ions (La(III), Pr(III), Ce(III), among others) (Teixeira *et al.*, 2017; Teixeira *et al.*, 2016a; Teixeira *et al.*, 2016b), further highlighting its versatility and potential in the development of novel coordination compounds.

The applications of both H-pABA and its coordination compounds extend beyond pharmaceutical contexts. Numerous studies have reported their use in various other fields, including UV ligh absorption, enabled by chromophoric groups such as benzene and carboxylate rings in their structure (Gómez *et al.*, 2020); their role as stabilizing agents in nanoparticle synthesis, preventing particle agglomeration (Susanthy *et al.*, 2020); and in the development of H-pABA-functionalized nanoparticles for the detection of explosive materials (Ghosh and Luwang, 2015), among other applications across diverse fields of research.

Several methods have been employed to characterize complexes synthesized with 4-aminobenzoic acid. For instance, Ye *et al.* (2004) synthesized complexes with H-pABA using terbium as the central ion and characterized them using spectroscopic techniques such as FTIR, PXRD, and fluorescence spectroscopy owing to their luminescent properties.

Furthermore, thermoanalytical techniques play a valuable role in characterizing coordination compounds by providing information on hydration water content, thermal stability, decomposition pathways, and sample purity, as demonstrated by Rodrigues *et al.* (2006) in their synthesis and characterization of a series of lanthanide complexes using 4-methoxybenzoate as a ligand.

Additionally, evolved gas analysis (EGA) can provide valuable insights into the thermal decomposition mechanisms of synthesized complexes. This technique involves identifying volatile products and gases released during the compound's combustion, making it a useful tool for material characterization (Teixeira *et al.*, 2022; Xie and Pan, 2001).

Considering its multifunctional character, capable of coordinating through both amino and carboxylate groups, H-pABA is a versatile ligand with well-known applications in its free form and coordination compounds, particularly in the biological field (Kalembkiewicz *et al.*, 2017; Olanrewaju *et al.*, 2018; Sapijanskaitė-Banevič *et al.*, 2021). However, despite the relevance of lanthanide complexes in several technological and biomedical applications, comprehensive thermoanalytical data on their *p*-aminobenzoate derivatives remain limited. Thorough characterization is a fundamental step before any application studies can be undertaken.

In this context, the present study aims to synthesize and conduct thermoanalytical and spectroscopic studies of Ho(III), Er(III), Tm(III), Yb(III), Lu(III), and Y(III) *p*-aminobenzoate complexes, with emphasis on their thermal behavior under oxidative and inert atmospheres. The study involves determining the metal-to-ligand stoichiometry, proposing coordination modes based on spectroscopic techniques, investigating thermal decomposition mechanisms through TG-DSC/FTIR analysis, and evaluating potential phase transitions using DSC analysis.

2. Experimental

For the synthesis, *p*-aminobenzoic acid (H-pABA) was obtained from Sigma-Aldrich with 99% purity and used without further purification.

The carbonates of heavy trivalent lanthanides (holmium, erbium, thulium, ytterbium, lutetium) and yttrium were prepared by the slow addition of a saturated sodium hydrogen carbonate solution, under continuous stirring, to the corresponding metal chlorides previously obtained, following the procedure described in the literature (Teixeira *et al.*, 2016b).

Solid-state holmium, erbium, thulium, ytterbium, lutetium, and yttrium complexes were obtained following the method reported by Teixeira, *et al.* (2016b). While stirring, a slight excess of the respective metal carbonate suspension was added to 50 mL of an aqueous suspension of *p*-aminobenzoic acid (0.15 mol L^{-1}). The aqueous suspension was then heated to boil until complete neutralization of the carbonate. The resulting solids were filtered and washed with ethanol and distilled water. They were then dried at 50 °C in a forced-air circulation oven for 12 h and kept in a desiccator over anhydrous calcium chloride.

The mass losses observed in the thermogravimetric (TG) curves were used to determine the contents of metal ions, hydration water, and *p*-aminobenzoate in the solid-state complexes. Metal ion concentrations were also determined by

complexometric titration with standard EDTA solution, following calcination of the samples to their respective oxides and dissolution in hydrochloric acid (Flaschka and Naiman, 1959).

Carbon, hydrogen, and nitrogen contents were analyzed using microanalytical procedures, with a CHN Elemental Analyzer (PerkinElmer, model 2400).

X-ray powder diffraction patterns were collected using a Siemens D-5000 X-ray diffractometer with CuKα radiation (λ=1.541 Å) and settings of 40 kV and 20 mA.

Fourier-transform infrared (FTIR) spectra were obtained using a Nicolet iS10 FTIR spectrophotometer with an ATR accessory featuring a Ge window. Each spectrum was acquired with 32 scans at a resolution of 4 cm^{-1}.

Simultaneous thermogravimetry–differential thermal analysis (TG–DTA) and differential scanning calorimetry (DSC) curves were obtained using two thermal analysis systems from TA Instruments: the SDT 2960 for TG–DTA and the Q10 for DSC. TG–DTA analyses were performed under two different atmospheres (air and nitrogen), both with a purge gas flow of 100 mL min^{-1}. At the same time, DSC measurements were conducted exclusively under nitrogen at the same flow rate. A heating rate of 10 °C min^{-1} was adopted for all analyses. Sample masses were approximately 7 mg for TG–DTA and 2 mg for DSC. TG–DTA measurements were applied using alumina crucibles, while DSC curves were obtained using aluminum crucibles with perforated lids. Sample masses for DSC and TG–DTA analyses were selected based on established literature protocols, considering the intrinsic sensitivity of each technique. Owing to its high sensitivity to enthalpic changes, DSC requires small sample amounts, whereas TG–DTA, being less sensitive, necessitates larger masses to ensure reliable detection of thermal events.

The identification of the main gaseous products released during the thermal decomposition (dry air atmosphere) and pyrolysis (N_2 atmosphere) of the complexes was carried out using a TG-DSC 1 Mettler Toledo coupled to a Nicolet FTIR spectrophotometer with gas cell and DTGS KBr detector. The TG-DSC furnace and heated gas cell (250 °C) were connected through a heated (225 °C) 120 cm stainless steel transfer line with a diameter of 3.0 mm, both purged with dry air and nitrogen (50 mL min^{-1}) and using a heating rate of 10 °C min^{-1}. The FTIR spectra were recorded with 16 scans per spectrum at a resolution of 4 cm^{-1}.

A generative artificial intelligence tool, ChatGPT, developed by OpenAI, was restricted used during the final revision of the manuscript to assist with English-language editing, grammatical correction, improvement of textual clarity, and organization of the responses to the editorial comments. Generative artificial intelligence was not used in the conception of the study, experimental procedures, generation or modification of data, calculations, analysis of results, preparation of figures, or formulation of scientific conclusions. All suggested changes were critically reviewed and approved by the authors and an English-language specialist, who assume full responsibility for the final manuscript.

3. Results and discussion

3.1. Analytical results and characterization

Thermoanalytical (TG) and analytical data (elemental analysis and EDTA complexometry) for the heavy trivalent lanthanide and yttrium *p*-aminobenzoate complexes are shown in Table 1. These data allowed the determination of the metal-*p*-ABA stoichiometry, the number of water molecules, and the metal content in these compounds, which are consistent with the general formula $[Ln(p\text{-}ABA)_3 \cdot H_2O]$ for the Ho(III), Er(III), Tm(III), Yb(III), and Y(III) compounds, and $[Ln(p\text{-}ABA)_3 \cdot 0.5H_2O]$ for the Lu(III) compound. In this formula, Ln represents the heavy trivalent lanthanide ions and yttrium, while *p*-ABA represents the *p*-aminobenzoate ligand.

Table 1. Analytical and thermoanalytical (TG*) data for the synthesized complexes.

Compounds		$Ho(p\text{-}ABA)_3 \cdot H_2O$	$Er(p\text{-}ABA)_3 \cdot H_2O$	$Tm(p\text{-}ABA)_3 \cdot H_2O$	$Yb(p\text{-}ABA)_3 \cdot H_2O$	$Lu(p\text{-}ABA)_3 \cdot 0.5H_2O$	$Y(p\text{-}ABA)_3 \cdot H_2O$
Final residue (%)	Calcd.	31.95	32.21	32.41	32.87	33.53	21.91
	EDTA	31.81	32.50	32.30	32.79	33.70	21.82
	TG	32.17	32.44	32.51	33.28	34.10	22.36
H-pABA Lost (%)	Calcd.	65.00	64.75	64.53	64.12	64.95	74.59
	TG	64.65	64.63	64.39	63.65	64.59	74.23
Water (%)	Calcd.	3.05	3.04	3.03	3.01	1.52	3.50
	TG	3.18	2.93	3.10	3.07	1.31	3.41
C (%)	Calcd.	42.65	42.48	42.36	42.07	42.61	48.94
	EA	42.51	42.34	42.30	41.81	42.24	48.66
	TG	42.94	42.70	42.10	42.39	42.35	48.50
N (%)	Calcd.	7.11	7.08	7.06	7.01	7.10	8.16
	EA	7.09	7.06	7.05	6.97	7.04	8.12
	TG	7.40	6.84	6.80	7.29	7.35	8.50
H (%)	Calcd.	3.42	3.40	3.39	3.37	3.24	3.92
	EA	3.41	3.39	3.38	3.35	3.21	3.90
	TG	3.66	3.29	3.51	3.51	3.30	4.15
Final Residue		Ho_2O_3	Er_2O_3	Tm_2O_3	Yb_2O_3	Lu_2O_3	Y_2O_3

Note: *p*-ABA = *p*-aminobenzoate, *TG in air atmosphere
Source: Elaborated by the authors.

https://doi.org/10.26850/1678-4618.eq.v51.2026.e1662

The X-ray powder diffraction patterns (Fig. 1) indicate that all complexes have a crystalline structure. Excluding the lutetium complex, the diffraction profiles of the remaining synthesized compounds suggest isomorphous structures.

The X-ray powder patterns of the compounds with isomorphous structures are consistent with the findings of Sun *et al.* (2004). The main Bragg peaks are observed at 7.78, 10.08, 14.96, 15.62, 20.16, 23.86, 24.24, 25.04, 31.12, 36.8, and 37.22° (2θ). According to the authors' results, these complexes probably exhibit a polymeric structure with a two-dimensional (2D) or binuclear array (Sun *et al.*, 2004).

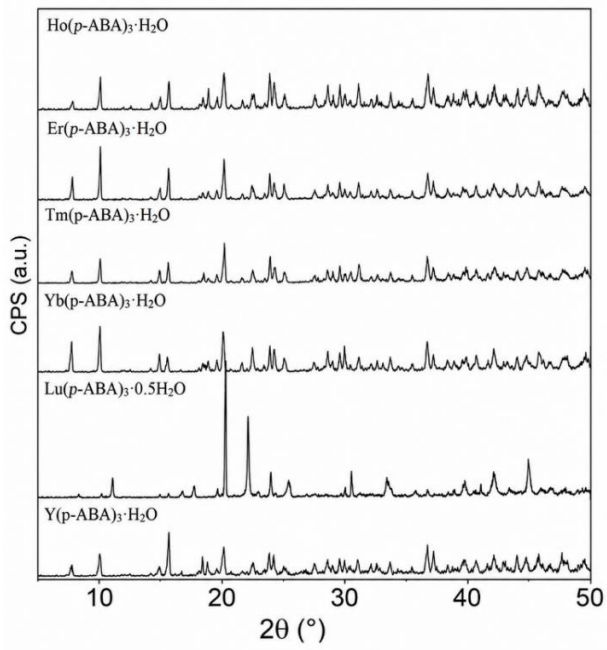

Figure 1. X-ray diffraction powder patterns for Ho(*p*-ABA)$_3$·H$_2$O, Er(*p*-ABA)$_3$·H$_2$O, Tm(*p*-ABA)$_3$·H$_2$O, Yb(*p*-ABA)$_3$·H$_2$O, Lu(*p*-ABA)$_3$·0.5H$_2$O and Y(*p*-ABA)$_3$·H$_2$O.
Source: Elaborated by the authors.

3.2. Thermal analysis

The thermal decomposition data (TG-DTA curves) of the synthesized compounds obtained from dry air and nitrogen atmospheres are presented in Fig. 2a and 2b, respectively. Compared with the same atmosphere, all heavy trivalent lanthanide and yttrium compounds exhibit a similar thermal behavior profile.

These curves exhibit mass losses in consecutive and/or overlapping steps, accompanied by corresponding thermal events or, in some cases, the absence of detectable thermal events.

In a dry air atmosphere, the thermal decomposition of all the compounds is complete by 680 °C, with the formation of their respective oxides, as shown in Table 1. Under a nitrogen atmosphere, mass loss is observed for all compounds up to 1000 °C, and at this temperature, the final residue is a mixture of carbonaceous material and lanthanide oxides.

The thermal stability of the synthesized compounds was evaluated under both atmospheric conditions and related to the ionic radius of each trivalent metal ion. The stability order is as follows:

Dry Air Atmosphere:

- Hydrated compounds: Lu > Er = Tm = Yb = Y > Ho
- Anhydrous compounds: Lu > Tm > Yb > Er > Y > Ho

Nitrogen Atmosphere:

- Hydrated compounds: Yb > Er = Lu > Ho = Tm = Y
- Anhydrous compounds: Lu > Er = Tm = Yb = Y > Ho

The smooth contraction of the ionic radius across the trivalent lanthanide series typically results in compounds with similar properties, including comparable thermal and thermodynamic behavior. However, in most cases, the stability constants increase progressively along the lanthanide series (Peters *et al.*, 2020).

For the synthesized complexes, especially the anhydrous ones, a non-linear increase in thermal stability with decreasing ionic radius is observed.

As previously mentioned, the similarity observed in the TG-DTA profiles of these complexes under air atmosphere is not reproduced in a nitrogen atmosphere. Consequently, the TG-DTA curves for each atmosphere are presented separately.

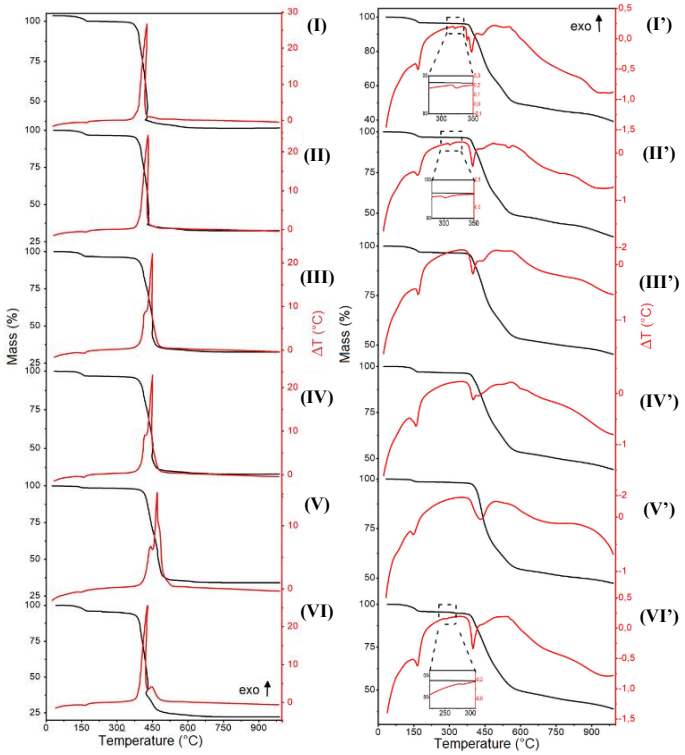

Figure 2. Simultaneous TG-DTA curves of the synthesized complexes under dynamic **(a)** dry air and **(b)** N_2^* atmospheres.
Source: Elaborated by the authors.

3.3. TG-DTA

3.3.1. Air atmosphere

The simultaneous TG-DTA curves of the heavy trivalent lanthanide and yttrium compounds obtained under a dry air atmosphere are presented in **Fig. 2a**. For all the compounds, thermal decomposition occurs in three steps.

The first mass-loss step observed in the TG-DTA curves indicates that dehydration occurs in a single step. According to the temperature range of mass loss, the water molecule is strongly bonded and can be associated with coordination water (Parmar *et al.*, 2014; Sun *et al.*, 2004). Dehydration occurs between 95–130 °C (Ho), 100–180 °C (Er), 100–175 °C (Tm), 100–170 °C (Yb), 110–160 °C (Lu), and 100–180 °C (Y), corresponding to endothermic peaks at 120, 170, 165, 160, 150, and 170 °C, respectively.

The mass loss percentages observed in the TG curves and the calculated values associated with the dehydration of these compounds are shown in **Table 1**. The experimental results agree with the loss of 1 H_2O (Ho, Er, Tm, Yb, Y) and 0.5 H_2O (Lu).

After dehydration, the compounds were thermally stable up to 348 °C (Ho), 355 °C (Er), 365 °C (Tm), 360 °C (Yb), 380 °C (Lu), and 350 °C (Y). Above these temperatures, mass loss occurred in two consecutive steps, with the first being fast thermal decomposition followed by a slower secondary mass loss process.

The first step occurs up to 430 °C (Ho), 435 °C (Er), 475 °C (Tm, Yb), 520 °C (Lu), and 490 °C (Y), with corresponding mass losses of 59.63, 60.69, 61.13, 60.28, 62.56, and 67.19%, respectively. These mass losses correspond to a large and sharp exothermic peak at 430 °C (Ho), 435 °C (Er), 455 °C (Tm, Yb), 470 °C (Lu), and 435 °C (Y), attributed to the oxidation of the organic matter from the *p*-ABA and/or the gaseous products released during thermal decomposition.

For the Tm(III), Yb(III), Lu(III), and Y(III) compounds, a shoulder in the described DTA peak was observed at 420 °C (Tm, Yb), 445 °C (Lu), and 450 °C (Y). These shoulders suggest overlapping decomposition reactions during this stage. At the end of this first step, carbonaceous material and carbonate derivatives are formed as residues (Nunes *et al.*, 2016). Tests with a hydrochloric acid solution on samples heated up to the temperature corresponding to the formation of this intermediate, as indicated by the TG-DTA curves, confirmed the evolution of carbon dioxide and the presence of carbonate derivatives.

The final step occurs slowly, between 430–625 °C (Ho), 435–635 °C (Er), 475–680 °C (Tm, Yb), 520–655 °C (Lu), and 490–680 °C (Y), with mass losses of 5.02, 4.04, 3.26, 3.37, 2.03, and 7.04%, respectively. These losses are attributed to the oxidation of carbonaceous material and the thermal decomposition of carbonate derivatives.

No thermal event in the DTA curves associated with this mass-loss step was observed, probably because the mass loss occurs slowly and the temperature difference does not reach the detection limit of the DTA sensor and/or due to the balance between endothermic (carbonate derivative thermal decomposition) and exothermic (carbonaceous material oxidation) reactions.

The total mass loss observed up to the final decomposition temperature of each compound is consistent with the formation of Ln_2O_3 (Ln = Ho, Er, Tm, Yb, Lu, and Y) as the final residue, as shown in **Table 1**.

3.3.2. Nitrogen atmosphere

The simultaneous thermogravimetry and differential thermal analysis (TG-DTA) curves obtained under an N_2 atmosphere are presented in **Fig. 2b**. Similar to the behavior observed under a dry air atmosphere, these curves also show that dehydration occurs in a single step for all compounds and that the atmosphere used does not interfere with the dehydration process.

The anhydrous compounds exhibit a thermal decomposition process that occurs in two or three consecutive and overlapping steps, accompanied by endothermic thermal events attributed to the pyrolysis of the compounds. Additionally, physical phenomena or the absence of detectable thermal events were observed in the DTA curves.

Two patterns of thermal behavior are observed up to 1000 °C. Firstly, a close similarity is noted in the TG profiles of holmium to thulium compounds (**Fig. 2b** (I'–III')). On the other hand, ytterbium, lutetium, and yttrium compounds display another set of similar TG profiles (**Fig. 2b** (IV'–VI')).

Thus, the thermal behavior of each of these compounds is discussed based on their similarities.

3.3.2.1. Holmium, erbium and thulium compounds

The TG-DTA curves of these compounds are shown in **Fig. 2b** (I'–VI'). The first mass-loss step occurs between 92–175 °C (Ho), 95–180 °C (Er), and 92–180 °C (Tm), corresponds to an endothermic event at 170 °C (Ho, Er) and 175 °C (Tm). This step is attributed to dehydration with the loss of 1 H_2O, as also observed in a dry air atmosphere (Calcd. = 3.05, 3.04, 3.03; TG = 3.16, 3.13, and 3.14%, respectively).

The anhydrous compounds are stable up to 365, 370, and 370 °C, respectively. Above these temperatures, mass losses occur in three consecutive steps, with the first two steps overlapping. The first two mass losses are observed between 365–470 °C and 470–575 °C (Ho), 370–475 °C and 475–570 °C (Er), 370–480 °C and 480–580 °C (Tm), with mass losses of 29.32% and 18.07% (Ho), 31.64% and 15.99% (Er), and 30.37% and 14.62% (Tm), respectively.

These mass-loss steps exhibit endothermic events in the DTA curves at 375/390 °C and 440 °C (Ho), 400/442 °C and 555 °C (Er), and 400 °C and 445 °C (Tm). These events are attributed to the pyrolysis of the compounds, resulting in the formation of a mixture of carbonaceous material and carbonate derivatives as intermediate residues.

The final step occurs slowly, with mass losses of 10.23% (Ho), 13.65% (Er), and 6.47% (Tm), and may present an endothermic event or not. This step is attributed to the pyrolysis of the carbonaceous residue and the decomposition of carbonate derivatives. For all compounds, mass loss continues up to 1000 °C.

3.3.2.2. Ytterbium, lutetium and yttrium compounds

As previously observed under an air atmosphere, the simultaneous TG-DTA curves under an N_2 atmosphere (**Fig. 2b** (IV'–VI')) show that dehydration occurs in a single mass-loss step between 107–175 °C (Yb), 95–170 °C (Lu), and 90–180 °C (Y), corresponding to endothermic peaks at 165, 150, and 170 °C, respectively. The percentage of mass loss observed during dehydration is consistent with the loss of 1 H_2O for ytterbium and yttrium compounds and 0.5 H_2O for the lutetium compound.

The anhydrous compounds are stable up to 370 °C (Yb, Y) and 380 °C (Lu). Unlike the Ho, Er, and Tm compounds, above this temperature, the thermal decomposition of these anhydrous compounds occurs in only two consecutive steps, with mass losses still being observed up to 1000 °C.

The first step, observed between 370–580 °C (Yb), 380–600 °C (Lu), and 370–585 °C (Y), results in mass losses of 42.84, 43.84, and 46.00%, respectively. These losses correspond to endothermic peaks in the DTA curves at 400 and 430 °C (Yb), 440 °C (Lu), and 400 °C (Y). These mass losses and thermal events are attributed to the pyrolysis of the compounds, leading to the formation of a mixture of carbonaceous material and carbonate derivatives.

The final step also occurs slowly, with mass losses of 10.11, 7.40, and 11.30%, respectively. These losses correspond to a smooth endothermic event between 600–800 °C (Lu), 870–1000 °C (Y), or no detectable thermal event (Yb). This step is attributed to the thermal decomposition of the intermediate residue formed in the previous step.

Additionally, the endothermic peaks observed in the DTA curves obtained under a nitrogen atmosphere at 324 °C (Ho), 303 °C (Er), and 290 °C (Y), as highlighted in **Fig. 2**, with no corresponding mass loss in the TG curves, are attributed to phase transformations.

3.4. DSC curves

The DSC curves of the synthesized complexes, under a dynamic nitrogen atmosphere up to 375 °C, are shown in **Fig. 3**. These curves display characteristic endothermic peaks, which are consistent with the thermal events observed in the DTA curves obtained under a nitrogen atmosphere, **Fig. 2b** (I', II' and VI').

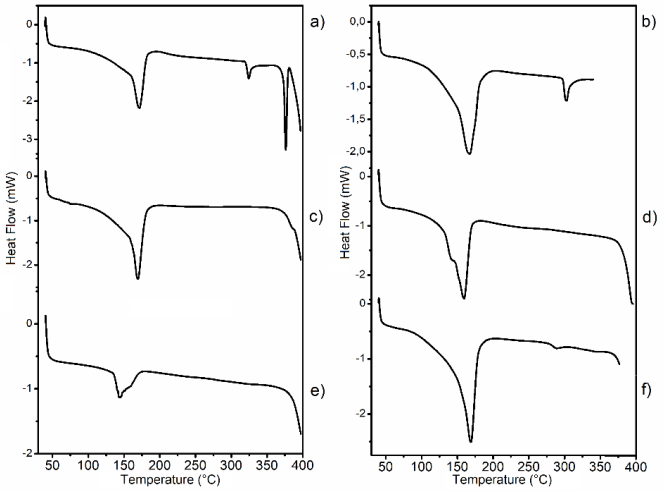

Figure 3. DSC curves for **(a)** Ho, **(b)** Er, **(c)** Tm, **(d)** Yb, **(e)** Lu and **(f)** Y synthesized complexes.
Source: Elaborated by the authors.

The endothermic peaks observed at 172 °C (Ho), 167 °C (Er), 170 °C (Tm), 160 °C (Yb), 143 °C (Lu), and 169 °C (Y) are attributed to dehydration. The dehydration enthalpies for these compounds were 75.0, 86.3, 76.6, 82.2, 19.6, and 94.6 kJ·mol^{-1}, respectively.

Small endothermic peaks observed in the DSC curves of the holmium, erbium, and yttrium complexes are attributed to reversible phase transformations and appear at 324, 303, and 290 °C, respectively. The phase transformation enthalpies were 4.1, 5.1, and 0.84 kJ·mol^{-1}, respectively. These phase transformations are likely associated with changes in the crystallinity of the compounds attributed to the formation of a new polymorphic form, as previously reported for other *p*-aminobenzoate lanthanide complexes (Teixeira *et al.*, 2016a; Teixeira *et al.*, 2016b).

The heating and cooling DSC curve of the erbium complex, representative of all compounds, confirms the reversibility of the phase transition (**Fig. 4**). During heating, the curve exhibits an endothermic peak at 303 °C, attributed to the phase transformation, and during cooling, an exothermic peak is observed at 229 °C. A second heating and cooling cycle was performed, and the endothermic (heating) and exothermic (cooling) peaks were again observed.

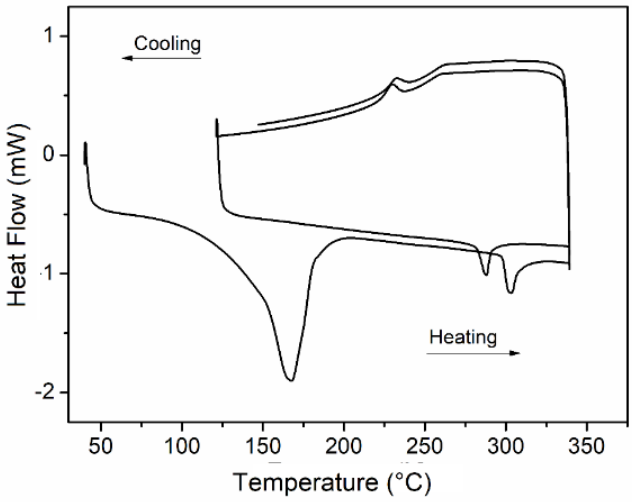

Figure 4. DSC heating and cooling curves of erbium complex.
Source: Elaborated by the authors.

The temperature difference between the peaks in the first and second heating and cooling cycles can be explained by the fact that, in the second cycle, the sample had already undergone a relaxation process during the first heating cycle.

3.5. Evolved gas analysis

Evolved gas analysis by TG-DSC/FTIR was employed to identify the main gaseous products released at different temperatures during the thermal decomposition of the complexes investigated in this study. **Figure 5a** and **b** show the FTIR spectra of the gases that evolved from the erbium complex at different temperatures.

Summary tables listing the gases identified under nitrogen and air atmospheres at different temperatures for all complexes, along with the FTIR spectra of the other compounds, are provided in the supplementary material.

The assignment of the leading bands observed in the FTIR spectra of the evolved gaseous products during thermal decomposition was based on the literature (Pavia *et al.*, 2010; Silverstein *et al.*, 2005; Teixeira *et al.*, 2016a; Teixeira and Siqueira, 2016) and the OMNIC software database.

https://doi.org/10.26850/1678-4618.eq.v51.2026.e1662

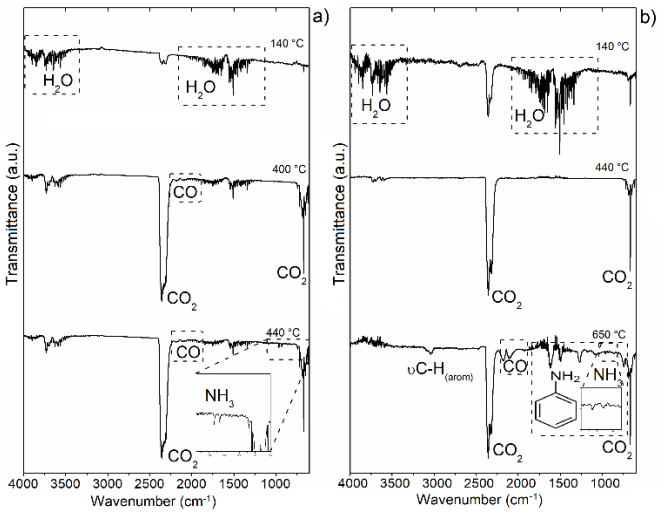

Figure 5. FTIR spectra from the gaseous products evolved during the thermal decomposition of the erbium complex in air **(a)** and nitrogen **(b)** atmospheres.
Source: Elaborated by the authors.

In both atmospheres, during the first mass loss step, bands were observed between 1300–2000 cm^{-1} and 3450–4000 cm^{-1}, characteristic of H_2O molecules from compound dehydration (Caires *et al.*, 2017; Pavia *et al.*, 2010; Silverstein *et al.*, 2005; Teixeira *et al.*, 2017). At 430 °C, CO_2 (bands at 2357 and 668 cm^{-1}), CO (bands at 2188 and 2106 cm^{-1}), and NH_3 (very weak bands at 968 and 929 cm^{-1}) were identified as the main gaseous products released during the thermal decomposition of the anhydrous compounds under a dry air atmosphere (**Fig. 5a**).

Aniline, CO_2, CO, and NH_3 were identified under an N_2 atmosphere (**Fig. 5b**). Aniline was characterized by the presence of bands at 3047 cm^{-1} (ν=C-H_aromatic), 1619/1501 cm^{-1} (νC=C), 1273 cm^{-1} (νC-N_amine), 875 cm^{-1} (βC-H_aromatic), and 744 cm^{-1} (βCCN). The absence of aniline in the gaseous products released during the thermal decomposition of the compounds under a dry air atmosphere suggests a different thermal decomposition mechanism between the studied atmospheres. This difference may be attributed to the high energy released during the thermal decomposition process under an oxidizing atmosphere, which promotes complete decomposition of aniline into smaller gaseous molecules such as CO_2, CO, and NH_3.

Under a dynamic N_2 atmosphere, due to the release of aniline and CO_2 as gaseous products, qualitative tests performed with hydrochloric acid and the mass value of the residue obtained until the end of the first (Ho, Er, and Tm) and second (Yb, Lu, and Y) steps of the thermal decomposition of anhydrous compounds (Calcd. = 43.11, 43.33, 43.21, 43.88, 44.72, and 34.71%; TG = 52.61, 52.37, 55.01, 57.16, 56.16, and 54.00%, respectively) suggest that, during this step, the breaking of the aromatic–COO–M bond coincides with thermal decomposition, This process results in the formation of a non-stoichiometric mixture of carbonaceous material and carbonate derivatives as supported by the TG-DTA results and previous observation in similar metal complexes (Caires *et al.*, 2017; Nunes *et al.*, 2016).

3.6. Infrared spectroscopy

FTIR spectra of H-pABA, sodium *p*-aminobenzoate, and their heavy trivalent lanthanide and yttrium complexes were recorded following the parameters described in the experimental section and are presented in **Fig. 6** and **Table 2**.

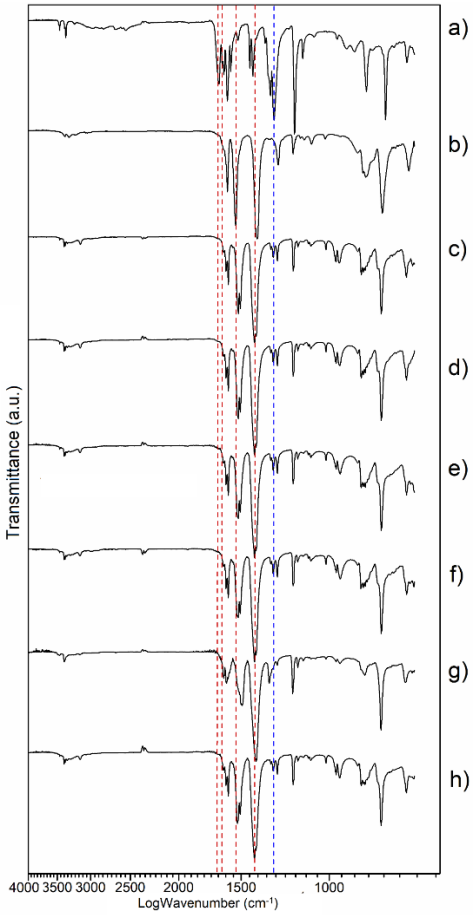

Figure 6. FTIR spectra of **(a)** H-pABA; **(b)** Na-pABA; **(c)** Ho(*p*-ABA)$_3$·H_2O; **(d)** Er(*p*-ABA)$_3$·H_2O; **(e)** Tm(*p*-ABA)$_3$·H_2O; **(f)** Yb(*p*-ABA)$_3$·H_2O; **(g)** Lu(*p*-ABA)$_3$·0.5H_2O and **(h)** Y(*p*-ABA)$_3$·H_2O.
Source: Elaborated by the authors.

Bands at 1289 cm^{-1} (νC-OH), 1662 cm^{-1} (νC=O_{dimer}), 3460 cm^{-1} (vassNH_2), 3363 cm^{-1} (νsymNH_2), 1623 cm^{-1} (δNH_2), 1072 cm^{-1} (δoutNH_2), 1310 cm^{-1} (νC-N), 1421 cm^{-1} (δOH), and 1173 cm^{-1} (δCC_{ar}) were observed in the H-pABA spectrum, in agreement with previously published literature (Murugavel *et al.*, 2000; Samsonowicz *et al.*, 2005b; Silva *et al.*, 2014; Teixeira, *et al.*, 2016a).

For Na-pABA and the synthesized complexes, the assignment of the main bands observed in the FTIR spectra obtained for the solid-state complexes is presented in **Table 2**. The band at 1622 cm^{-1}, attributed to the C=O stretching of the H-pABA dimer, was not observed in the spectra of the sodium salt and trivalent lanthanide and yttrium compounds.

In contrast, the FTIR spectra showed very strong bands attributed to the asymmetrical and symmetrical stretching of the carboxylate group, observed in the regions 1492–1538 cm^{-1} and 1398–1410 cm^{-1}, respectively. See the exact wavenumbers for each band in **Table 2**. The changes observed in these bands indicate that the carboxylate group participates in metal-*p*-ABA coordination. The coordination mode of the carboxylate group with the metal ion has been determined in several studies by correlation of the difference between the asymmetrical (vasCOO^-) and symmetrical stretching (vsCOO^-) frequencies of the carboxylate group bands in the metal complexes with the corresponding difference observed for the sodium salt ligand, using the **Eq. 1** (Deacon and Phillips, 1980; Zeleňák *et al.*, 2007).

$$\Delta\nu_{COO^-} = \text{vas}COO^- - \text{vs}COO^- \quad (1)$$

For this series of synthesized metal complexes, the $\Delta\nu_{COO^-}$ values were calculated based on the band positions of the carboxylate group, according to the wavenumbers observed in the FTIR spectra provided in **Table 2**. $\Delta\nu_{COO^-}$ values ranging from 94 to 127 cm^{-1} were observed for metal complexes, while for the sodium salt, $\Delta\nu$ was 140 cm^{-1} (**Table 2**). Except for the lutetium complex, the $\Delta\nu_{COO^-}$ values found and the existence of two asymmetrical and symmetrical carboxylate stretches suggest a bidentate bridging and/or chelating interaction of the carboxylate group of the *p*-ABA with the metal ions, indicating two distinct modes of carboxylate binding (Zeleňák *et al.*, 2007).

In case of lutetium complex, the $\Delta\nu COO^-$ value suggests a bidentate chelating coordination of the carboxylate group, since $\Delta\nu_{complex}$ (94) << $\Delta\nu_{sodium\ salt}$ (140).

The band positions characteristic of the amino group was also red-shifted when the FTIR spectra of the Ho–Yb and Y metal complexes were compared to those of the free ligand (H-pABA) and the sodium salt (Na-pABA) (**Table 2**). These shifts suggest an interaction between the amino group of the *p*-ABA and the metal ions, as previously reported in the literature for other *p*-aminobenzoate complexes. This finding supports the proposed 2D polymeric or double nuclear structure for the Ho – Yb and Y synthesized complexes, where the *p*-ABA exhibits three different coordination modes (Sun *et al.*, 2004).

Table 2. Wavenumbers (cm^{-1}) and assignments of main bands occurring in the FTIR spectra of Ho, Er, Tm, Yb, Lu and Y complexes in comparison with *p*-aminobenzoic acid, sodium *p*-aminobenzoate.

Assignments	Wavenumbers (cm^{-1})							
	H-pABA	Na(*p*-ABA)	Ho(*p*-ABA)$_3$·H_2O	Er(*p*-ABA)$_3$·H_2O	Tm(*p*-ABA)$_3$·H_2O	Yb(*p*-ABA)$_3$·H_2O	Lu(*p*-ABA)$_3$·0.5H_2O	Y(*p*-ABA)$_3$·H_2O
$\nu asNH_2$	3460_w	3377_w	3390_{vw}	3390_{vw}	3390_{vw}	3390_{vw}	3388_{vw}	3390_{vw}
νsNH_2	3363_w	3315_w	3373_{vw}	3374_{vw}	3375_{vw}	3375_{vw}	overlapped	3374_{vw}
νOH	$3000\text{-}2500_w$	3223_w	3289_{vw}	3289_{vw}	3293_{vw}	3293_{vw}	3231_{vw}	3290_{vw}
νCH	$3010\text{-}3050_w$	$3045;3012_w$	3145_{vw}	3147_{vw}	3150_{vw}	3152_{vw}	3158_{vw}	3148_{vw}
N-H···O/O-H···N	$2300\text{-}3000_w$							
$\nu C{=}O$	1663_s							
$\delta NH_2{+}\nu C{=}C$	1623_m	overlapped	overlapped	overlapped	overlapped	overlapped	1624_w	1627_w
$\nu C{=}C$	1598_s	1598_m	1592_m	1591_m	1592_s	1592_s	1605_s	1608_m
$\nu C{=}C{+}\delta OH_{H2O}$	1574_m							
$vasCOO^-$		1538_{vs}	$1520;1506_{vs}$	$1520;1507_{vs}$	$1520;1507_{vs}$	$1520;1507_{vs}$	1492_{vs}	$1526;1507_{vs}$
$\nu C{=}C$	1441_m							
δOH	1421_m							
$vsCOO^-$		1398_{vs}	$1410;1399_{vs}$	$1410;1399_{vs}$	$1410;1399_{vs}$	$1410;1400_{vs}$	1398_{vs}	$1410;1399_{vs}$
$\nu C{-}N$	1310_s	1264_m	1293_w	1293_w	1294_w	1294_w	1318_s	1293_w
$\nu C{-}OH$	1289_{vs}							
$\delta_{out}NH_2$	1072_{vw}	1084_m	1087_{vw}	1088_{vw}	1087_{vw}	1087_{vw}		1088_{vw}
δCH	1177_m	1180_w	1179_m	1180_m	1180_m	1180_m	1182_s	1180_s
$\delta_{out}CH$	842_m	845_m	862_m	862_m	863_m	863_m	848_s	862_m
$\delta_{out}CH$	770_{va}	782_{vs}	786_{vs}	786_{vs}	786_{vs}	786_m	787_{vs}	787_{vs}
$\delta C\text{-}C\text{-}C$	699_w	692_m	700_m	700_m	700_m	699_w	703_w	700_w
$\Delta vas_{COO^-} - vs_{COO^-}$	-	140	121;96	121;97	121;97	120;97	94	127;97

Source: Elaborated by the authors.

For the lutetium complex, the $\nu C{-}N$ band position attributed to the amino group was blue-shifted from 1310 to 1318 cm^{-1} compared to that of H-pABA. Additionally, the N–H stretching and bending modes also exhibited changes or were overlapped, which can be attributed to hydrogen bonding between the free N–H group and oxygen atoms (Sun *et al.*, 2004; Tsaryuk *et al.*, 2014). These results suggest that the N atoms of *p*-aminobenzoate are not coordinated in the lutetium complex.

The difference observed in the coordination mode of the lutetium complex, in contrast to the other synthesized lanthanide complexes, can be associated with its smaller ionic radius (Sun *et al.*, 2004). There is probably only enough space for half of the water molecules, and not enough room around the Lu^{3+} ion to allow coordination with the nitrogen atom of the amino group.

4. Conclusions

Heavy trivalent lanthanide *p*-aminobenzoate complexes were synthesized by reacting the ligand (H-pABA) with the corresponding metal carbonates (Ho(III), Er(III), Tm(III), Yb(III), Lu(III), and Y(III)). The combination of analytical, thermoanalytical, and spectroscopic methods supported the successful synthesis of these complexes. The TG curves, CNH analysis, and complexometry with EDTA of these compounds allowed the establishment of the general formula [Ln(*p*-ABA)$_3$·H_2O] for the Ho(III), Er(III), Tm(III), Yb(III), and Y(III) compounds, and [Ln(*p*-ABA)$_3$·0.5H_2O] for the Lu(III) compound, where Ln represents heavy trivalent lanthanide ions and yttrium, and *p*-ABA is the *p*-aminobenzoate ligand. Furthermore, the TG-DTA curves provided previously unreported information about the thermal decomposition of these complexes under oxidative and pyrolytic conditions.

X-ray diffractometry shows that all synthesized complexes have a crystalline structure. Except for the lutetium complex, all others exhibit evidence of isomorphous structures. Evolved gas analysis by TG-DSC/FTIR allowed the determination of the main gaseous products released during the thermal decomposition of the complexes in both atmospheres studied. Additionally, TG-DSC/FTIR data contributed to understanding the thermal decomposition mechanism of these complexes.

From DSC analysis, it was possible to determine the enthalpies of dehydration and study the phase transition observed during the heating of the holmium, erbium, and yttrium complexes.

FTIR spectroscopic data indicated that, except for the lutetium complex, the coordination of *p*-aminobenzoate with the metal ions occurs through both the carboxylate and amino groups. In the lutetium complex, coordination occurs only through the carboxylate group, which binds in a bidentate chelating mode. In

contrast, the other complexes show coordination involving the NH_2 group and two distinct carboxylate binding modes.

Authors' contribution

Conceptualization: José Augusto Teixeira; Ana Paula Segantin Gaspari Giovanini; Guilherme Isquibola; Flávio Junior Caires; **Data Curation:** José Augusto Teixeira; Ana Paula Segantin Gaspari Giovanini; Flávio Junior Caires; **Formal analysis:** José Augusto Teixeira; Guilherme Isquibola; **Funding acquisition:** Flávio Junior Caires; José Augusto Teixeira; **Investigation:** José Augusto Teixeira; Ana Paula Segantin Gaspari Giovanini; Flávio Junior Caires; Guilherme Isquibola; **Methodology:** José Augusto Teixeira; Ana Paula Segantin Gaspari Giovanini; Flávio Junior Caires; Guilherme Isquibola; **Project administration:** José Augusto Teixeira; Ana Paula Segantin Gaspari Giovanini; Flávio Junior Caires; Guilherme Isquibola; **Resources:** José Augusto Teixeira; Ana Paula Segantin Gaspari Giovanini; Flávio Junior Caires; **Software:** Not applicable; **Supervision:** José Augusto Teixeira; Flávio Junior Caires; **Validation:** José Augusto Teixeira; Ana Paula Segantin Gaspari Giovanini; Flávio Junior Caires; Guilherme Isquibola; **Visualization:** José Augusto Teixeira; Ana Paula Segantin Gaspari Giovanini; Flávio Junior Caires; Guilherme Isquibola; **Writing – Original Draft:** José Augusto Teixeira; Ana Paula Segantin Gaspari Giovanini; Flávio Junior Caires; Guilherme Isquibola; **Writing – Review & Editing: José** Augusto Teixeira; Ana Paula Segantin Gaspari Giovanini; Flávio Junior Caires; Guilherme Isquibola.

Conflict of interest

The authors declare that there is no conflict of interest involving this manuscript.

Data availability statement

All data sets were generated or analyzed in the current study.

Artificial Intelligence usage statement

ChatGPT, a generative artificial intelligence tool developed by OpenAI, was used exclusively during the final editorial revision of the manuscript to assist with English-language editing, grammatical correction and textual clarity.

Funding

Fundação de Amparo à Pesquisa do Estado de São Paulo (FAPESP), https://doi.org/10.13039/501100001807, Grant No. 2023/06756-1;

Conselho Nacional de Desenvolvimento Científico e Tecnológico (CNPq), https://doi.org/10.13039/501100003593, Grant Nos. 317282/2021-2 and 443152/2024-1;

Coordenação de Aperfeiçoamento de Pessoal de Nível Superior (CAPES), https://doi.org/10.13039/501100002322.

Acknowledgments

Not applicable.

References

Akberova, S. I. New Biological Properties of *p*-Aminobenzoic Acid. *Biology Bulletin.* **2002**, *29* (4), 390–393. https://doi.org/10.1023/A:1016871219882

Aquaroni, N. A. S.; Nakahata, D. H.; Lazarini, S. C.; Resende, F. A.; Cândido, A. L. P.; da Silva Barud, H.; Claro, A. M.; de Carvalho, J. E.; Ribeiro, C. M.; Pavan, F. R.; Lustri, B. C.; Ribeiro, T. R. M.; Moreira, C. G.; Cândido, T. Z.; Lima, C. S. P.; Ruiz, A. L. T. G.; Corbi, P. P.; Lustri, W. R. Antibacterial Activities and Antiproliferative Assays over a Tumor Cells Panel of a Silver Complex with 4-Aminobenzoic Acid: Studies In Vitro of Sustained Release Using Bacterial Cellulose Membranes as Support. *Journal of Inorganic Biochemistry.* **2020**, *212,* 111247. https://doi.org/10.1016/j.jinorgbio.2020.111247

Caires, F. J.; Nunes, W. D. G.; Gaglieri, C.; Do Nascimento, A. L. C. S.; Teixeira, J. A.; Zangaro, G. A. C.; Treu-Filho, O.; Ionashiro, M. Thermoanalytical, Spectroscopic and DFT Studies of Heavy Trivalent Lanthanides and Yttrium(III) with Oxamate as Ligand. *Materials Research.* **2017**, *20* (4), 937–944. https://doi.org/10.1590/1980-5373-mr-2016-0633

Deacon, G. B.; Phillips, R. J. Relationships between the carbon-oxygen stretching frequencies of carboxylato complexes and the type of carboxylate coordination. *Coordination Chemistry Reviews.* **1980,** *33*, 227–250. https://doi.org/10.1023/A:1016871219882

Flaschka, H. A.; Naiman, B. EDTA Titrations: An Introduction to Theory and Practice. *Journal of The Electrochemical Society.* **1959**, *106* (8), 226C. https://doi.org/10.1149/1.2427458

Galbinur, T.; Obolensky, A.; Berenshtein, E.; Vinokur, V.; Chowers, I.; Chevion, M.; Banin, E. Effect of para-aminobenzoic acid on the course of retinal degeneration in the rd10 mouse. *Journal of Ocular Pharmacology and Therapeutics.* **2009**, *25* (6), 475–482. https://doi.org/10.1089/jop.2009.0020

Ghosh, D.; Luwang, M. N. *p*-Aminobenzoic acid (pABA) sensitization of $LaF_3:Tb^{3+}$ nanoparticles and its applications in the detection of explosive materials. *RSC Advances.* **2015**, *5*, 10468–10478. https://doi.org/10.1039/C4RA15304A

Gómez, N. A. G.; Silva, G. M.; Wilhelm, H. M.; Wypych, F. Zn_2Al Layered Double Hydroxides Intercalated with Nitrate and *p*-Aminobenzoate as Ultraviolet Protective Agents in Low-Density Polyethylene Nanocomposites and Natural Insulating Oils. *Journal of the Brazilian Chemical Society*. **2020** *31* (5), 971–981. https://doi.org/10.21577/0103-5053.20190262

Horozić, E.; Ademović, Z.; Suljagić, J.; Cipurković, A.; Rosa, E.; Sejfić, A.; Husejnagić, D.; Hodzić, S. Synthesis, spectral characterization, antibacterial and antifungal activity of copper (II)-pABA complex. *Technologia Acta.* **2019**, *12* (1), 27–30. https://doi.org/10.5281/zenodo.3268784

Jesty, T.; Ambili, K. S.; Baby, A. M.; Sonyamol, S. Characterization and optical studies of hybrid materials synthesized by covalently linking Eu^{3+} ions, para-aminobenzoic acid, and titania. *Journal of Applied Spectroscopy.* **2017**, *84* (1), 156-161. https://doi.org/10.1007/s10812-017-0444-0

Kalembkiewicz, J.; Kosińska, M.; Zapała, L. Complexes of aminobenzoic acids: A comprehensive review concerning synthesis, physical chemistry, structure and application. *Coordination Chemistry Reviews.* **2017**, *348*, 25–53. https://doi.org/10.1016/j.ccr.2017.07.004

Koma, D.; Yamanaka, H.; Moriyoshi, K.; Sakai, K.; Masuda, T.; Sato, Y.; Toida, K.; Ohmoto, T. Production of *p*-Aminobenzoic acid by metabolically engineered Escherichia coli. *Bioscience, Biotechnology, and Biochemistry.* **2014**, *78* (2), 350-357. https://doi.org/10.1080/09168451.2014.878222

LeBlanc, J. G.; Milani, C.; de Giori, G. S.; Sesma, F.; van Sinderen, D.; Ventura, M. Bacteria as vitamin suppliers to their host: A gut microbiota perspective. *Current Opinion in Biotechnology.* **2013**, *24* (2), 160–168. https://doi.org/10.1016/j.copbio.2012.08.005

Murugavel, R.; Karambelkar, V. V.; Anantharaman, G. Synthetic, spectroscopic and structural studies on 4-aminobenzoate complexes of divalent alkaline earth metals: X-ray crystal structures of $[\{Mg(H_2O)_6\}(4\text{-aba})_2]\cdot 2H_2O$ and $[Ca(H_2O)_2(4\text{-aba})_2]$ (4-aba=4-aminobenzoate). *Indian Journal of Chemistry - Section A Inorganic, Physical, Theoretical, and Analytical Chemistry.* **2000**, *39* (8), 843–850. https://doi.org/10.1021/ic990895k

Nunes, W. D. G.; Teixeira, J. A.; do Nascimento, A. L. C. S.; Caires, F. J.; Ionashiro, E. Y.; Ionashiro, M. A comparative study on thermal behavior of solid-state light trivalent lanthanide isonicotinates in dynamic dry air and nitrogen atmospheres. *Journal of Thermal Analysis and Calorimetry.* **2016**, *125* (1), 397–405. https://doi.org/10.1007/s10973-016-5339-4

Olanrewaju, A. A.; Ibeji, C. U.; Fabiyi, F.; Ibeji, C. U.; Fabiyi, F. S. Synthesis, Characterization, and Computational Studies of Metal(II) Complexes Derived from β-diketone and Para-aminobenzoic Acid Corrosion inhibition View project Mechanistic chemistry View project Synthesis, Characterization, and Computational Studies of Metal(II) Complexes Derived from β-diketone and Para-aminobenzoic Acid. *Indian Journal of Heterocyclic Chemistry*. **2018**, *28* (3), 351–361.

Parmar, B.; Bisht, K. K.; Maiti, P.; Paul, P.; Suresh, E. Syntheses, characterization and crystal structures of potassium and barium complexes of a Schiff base ligand with different anions. *Journal of Chemical Sciences.* **2014**, *126* (5), 1373–1384. https://doi.org/10.1007/s12039-014-0701-1

Pavia, D. L.; Lampman, G. M.; Kriz, G. S.; Vyvyan, J. R. Introdução à *Espectroscopia,* Tradução da 4ª Edição norte-americana; *Cengage* Learning, 2010.

Peters, J. A.; Djanashvili, K.; Geraldes, C. F. G. C.; Platas-iglesias, C. The chemical consequences of the gradual decrease of the ionic radius along the Ln-series. *Coordination Chemistry Reviews.* **2020**, *406*, 213146. https://doi.org/10.1016/j.ccr.2019.213146

Rodrigues, E. C.; Siqueira, A. B.; Ionashiro, E. Y.; Bannach, G.; Ionashiro, M. Synthesis, characterization, and thermal behaviour of solid 4-methoxybenzoates of heavier trivalent lanthanides. *Thermochimica Acta.* **2006**, *451* (1–2), 149–155. https://doi.org/10.1016/j.tca.2006.09.014

Rosbottom, I.; Ma, C. Y.; Turner, T. D.; O'Connell, R. A.; Loughrey, J.; Sadiq, G.; Davey, R. J.; Roberts, K. J. Influence of Solvent Composition on the Crystal Morphology and Structure of *p*-Aminobenzoic Acid Crystallized from Mixed Ethanol and Nitromethane Solutions. *Crystal Growth and Design.* **2017**, *17* (8), 4151–4161. https://doi.org/10.1021/acs.cgd.7b00425

Samsonowicz, M.; Hrynaszkiewicz, T.; Świsłocka, R.; Regulska, E.; Lewandowski, W. Experimental and theoretical IR, Raman, NMR spectra of 2-, 3- and 4-aminobenzoic acids. *Journal of Molecular Structure.* **2005**, *744–747,* 345–352. https://doi.org/10.1016/j.molstruc.2004.11.063

Sapijanskaitė-Banevič, B.; Palskys, V.; Vaickelionienė, R.; Šiugždaitė, J.; Kavaliauskas, P.; Grybaitė, B.; Mickevičius, V. Synthesis and antibacterial activity of new azole, diazole and triazole derivatives based on *p*-aminobenzoic acid. *Molecules.* **2021**, *26* (9), 2597. https://doi.org/10.3390/molecules26092597

Silva, R. C.; Caires, F. J.; Gomes, D. J. C.; Colman, T. A. D.; Ionashiro, M. Synthesis, characterization, and thermal study of solid-state alkaline earth metal mandelates, except beryllium and radium. *Journal of Thermal Analysis and Calorimetry.* **2014**, *117*, 217–221. https://doi.org/10.1007/s10973-014-3694-6

Silverstein, R. M.; Webster, F. X.; Kiemle, D. *Spectrometric Identification of Organic Compounds,* 7th Edition; Wiley, 2005. https://books.google.com/books?id=mQ8cAAAAQBAJ&pgis=1

Sowinska, M.; Morawiak, M.; Bochyńska-Czyż, M.; Lipkowski, A. W.; Ńska, E. Z.; Zabłocka, B.; Urbanczyk-Lipkowska, Z. Molecular antioxidant properties and in vitro cell toxicity of the *p*-aminobenzoic acid (PABA) functionalized peptide dendrimers. *Biomolecules.* ***2019***, *9* (3), 89. https://doi.org/10.3390/biom9030089

Sun, H. L.; Ye, C. H.; Wang, X. Y.; Li, J. R.; Gao, S.; Yu, K. B. Lanthanide contraction and pH value controlled structural change in a series of rare earth complexes with *p*-aminobenzoic acid. *Journal of Molecular Structure.* **2004**, *702* (1–3), 77–83. https://doi.org/10.1016/j.molstruc.2004.06.013

Susanthy, D.; Santosa, S. J.; Kunarti, E. S. Antibacterial activity of silver nanoparticles capped by *p*-aminobenzoic acid on Escherichia coli and Staphylococcus aureus. *Indonesian Journal of Chemistry.* **2020**, *20* (1), 182–189. https://doi.org/10.22146/ijc.44652

Teixeira, J. A.; Siqueira, A. B. Thermal and spectroscopic characterization, antioxidant evaluation and pyrolysis of losartan with some bivalent metals. *Journal of Analytical and Applied Pyrolysis.* **2016**, *117*, 17–24. https://doi.org/10.1016/j.jaap.2015.12.023

Teixeira, J. A.; Nunes, W. D. G.; Colman, T. A. D.; Do Nascimento, A. L. C. S.; Caires, F. J.; Campos, F. X.; Gálico, D. A.; Ionashiro, M. Thermal and spectroscopic study to investigate *p*-aminobenzoic acid, sodium *p*-aminobenzoate and its compounds with some lighter trivalent lanthanides. *Thermochimica Acta.* **2016a**, *624*, 59–68. https://doi.org/10.1016/j.tca.2015.11.023

Teixeira, J. A.; Nunes, W. D. G.; do Nascimento, A. L. C. S.; Colman, T. A. D.; Caires, F. J.; Gálico, D. A.; Ionashiro, M. Synthesis, thermoanalytical, spectroscopic study and pyrolysis of solid rare earth complexes (Eu, Gd, Tb and Dy) with *p*-aminobenzoic acid. *Journal of Analytical and Applied Pyrolysis.* **2016b**, *121*, 267–274. https://doi.org/10.1016/j.jaap.2016.08.006

Teixeira, J. A.; Nunes, W. D. G.; Fernandes, R. P.; do Nascimento, A. L. C. S.; Caires, F. J.; Ionashiro, M. Thermal behavior in oxidative and pyrolysis conditions and characterization of some metal *p*-aminobenzoate compounds using TG–DTA, EGA and DSC-photovisual system. *Journal of Analytical and Applied Pyrolysis.* **2017**, *128*, 261–267. https://doi.org/10.1016/j.jaap.2017.10.002

Teixeira, J. A.; Fernandes, R. P.; Isquibola, G.; Gaspari, A. P. S.; Machado, A. E. H.; Caires, F. J.; Ionashiro, M. Synthesis, thermal behavior in oxidative and pyrolysis conditions, spectroscopic and DFT studies of some alkaline earth metals *p*-aminobenzoate complexes using TG-DTA, DSC, PXRD and EGA (TG-FTIR) techniques. *Thermochimica Acta.* **2022**, *711*, 179184. https://doi.org/10.1016/j.tca.2022.179184

Tsaryuk, V.; Vologzhanina, A.; Zhuravlev, K.; Kudryashova, V.; Szostak, R.; Zolin, V. Structures and manifestation of ortho-, meta-, and para-NH_2-substitution in the optical spectra of europium and terbium aminobenzoates. *Journal of Photochemistry and Photobiology A: Chemistry*. **2014**, *285*, 52–61. https://doi.org/10.1016/j.jphotochem.2014.04.014

Xie, W.; Pan, W. P. Thermal characterization of materials using evolved gas analysis. *Journal of Thermal Analysis and Calorimetry.* **2001**, *65* (3), 669–685. https://doi.org/10.1023/A:1011946707342

Ye, C. H.; Sun, H. L.; Wang, X. Y.; Li, J. R.; Nie, D. B.; Fu, W. F; Gao, S. Preparation of three terbium complexes with *p*-aminobenzoic acid and investigation of crystal structure influence on luminescence property. *Journal of Solid State Chemistry.* **2004**, *177* (10), 3735–3742. https://doi.org/10.1016/j.jssc.2004.06.038

Zeleňák, V.; Vargová, Z.; Györyová, K. Correlation of infrared spectra of zinc(II) carboxylates with their structures. *Spectrochimica Acta - Part A: Molecular and Biomolecular Spectroscopy.* **2007**, *66* (2), 262–272. https://doi.org/10.1016/j.saa.2006.02.050

Zhai, L.; Zhang, W.-W.; Ren, X.-M.; Zuo, J.-L. Luminescent lanthanide MOFs based on conjugated 1,1′-ethynebenzene-3,3′,5,5′-tetracarboxylate ligand: syntheses, structures and photoluminescent properties. *Dalton Trans.* **2015**, *44*, 5746-5754. https://doi.org/10.1039/C4DT03794D